



Research paper

Heat transfer characteristics of methane-air diffusion flames impinging normally on plane surfaces

Satyananda Tripathy^a, Manmatha K. Roul^{b,*} and Akshaya Ku. Rout^b

^aSchool of Mechanical Engineering, KIIT University, Bhubaneswar, 751024, India

^bDepartment of Mechanical Engineering., GITA, Bhubaneswar, 752054, India

Article info:

Article history:

Received: 04/08/2018
Revised: 11/06/2019
Accepted: 13/06/2019
Online: 15/06/2019

Keywords:

Diffusion flame;
Heat transfer;
Equivalence ratio;
Nusselt number;
Reynolds number.

*Corresponding author:

mkroul@gmail.com

Abstract

Theoretical investigation of turbulent flame impinging normally on plane surfaces is done to determine the average Nusselt number and the plate heat flux distribution as functions of jet Reynolds number, equivalence ratio, and separation distance. The analysis is established on the mathematical formulation of the governing equations for conservation of mass, momentum, and energy. The turbulence phenomenon is analyzed with the help of the RNG $k-\varepsilon$ turbulence model. The radiative heat transfer model has been designed by using the Discrete Ordinates radiation model. Results show that the heat flux gradually increases with the radial distance towards the plate center and attains a maximum value at a location slightly away from the stagnation point. The peak value in the local heat flux comes closer to the stagnation point when the height between the plates and the nozzle increases. Effects of variation of dimensionless separation distance on heat transfer characteristics are investigated. It is observed that heat flux gradually improves when the value of separation distance changes from 12 to 8 and decreases near the stagnation region with the further decrease in separation distance from 8 to 4.

1. Introduction

The application of flame jets has been found in several industries to achieve a better heat transfer coefficient and to produce high rates of heat transfer. Heating by flames in industrial furnaces is employed to increase heat flux and thereby reduce fuel consumption significantly. So it is used for various works such as internal combustion engines, cooling and combustion in gas turbine engines, heating of boiler, the

formation of glass in the industries, and melting and surface treatment of metals. The lack of uniformity of heat flow near the stagnation point is a major drawback of the flame impingement heating process.

The heat transfer caused by the flame depends on the flame configuration, the temperature profile near the target plate, and the convection and radiation properties of components. The flame temperature depends on the structure of the impinging jet, which includes the wall jet

region, free jet region, and stagnation region, as shown in Fig. 1. Flame jet interaction with the ambient air at the outlet of the nozzle results in the growth of a non-uniform velocity profile in free jet region.

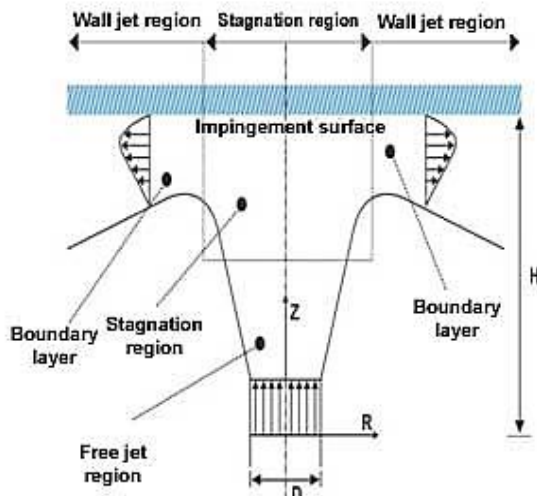


Fig. 1. Schematic diagram of flame impingement.

In the stagnation region, the static pressure is more than ambient pressure as a result of which the pressure gradients in the stagnation region suppresses the flow in the axial direction because the flame turns in the radially outward direction. The wall jet region is free from the mean pressure gradient.

Many researchers have investigated the flame impingement heat transfer experimentally and reported heat flux characteristics of methane-air flames impinging normally on target plates for various operating conditions. Baukal and Gebhart [1] reported that heat flux distribution on the plate surface due to flame impingement is non-uniform, and the peak value of heat flux was observed to have occurred not exactly at the stagnation point but a little away from it.

Boke et al. [2] investigate experimentally as well as theoretically the heat transfer phenomena using the $k-\epsilon$ turbulent model for modeling the turbulence phenomena in the combustor. For modeling the radiative heat transfer, they have used the discrete ordinates (DO) radiation model. Chander and Ray [3] observed that when the inner zone length is less as compared to the distance between target plate

and nozzle, peak heat flux increases when the Reynolds number increases. The majority of the studies using impinging flames for plane surfaces are carried out by Cornaro et al. [4] but the surface curvature effect of the target plate has not been investigated at all. Dong et al. [5] proposed correlation for Nusselt number as a function of different geometrical and operational parameters. Hou and Ko [6] investigated heat transfer due to impinging flames on inclined plates and observed that the plate temperature and efficiency depend strongly on the plate separation distance.

Kuntikana and Prabhu [7] compared the heat transfer phenomena of premixed flame jets and isothermal air jets with a variation of jet Reynolds number to the target surface, which is cooled from the opposite side. Agrawal et al. [8] studied the effect of impinging turbulent flames on inclined surfaces and found that when the oblique angle decreases, the distribution of heat flux in the lower part of the plate increases. But in the uphill part, it is slightly dependent on the oblique angle. The influence of convex curvature on heat transfer characteristic from an axisymmetric jet is studied by Lee et al. [9] and found that at the stagnation point, the Nusselt number increases with d/D .

Tripathy et al. [10] investigated theoretically diffusion as well as premixed flames impinging normally and obliquely on plane surfaces and found that the average Nusselt number over the plate increases when Re and ER increases and H/d decreases for both the flames.

Mirmohammadi and Ommi [11] numerically studied the internal combustion diesel engines using $k-\epsilon$ turbulence models and observed that both linear and nonlinear $k-\epsilon$ turbulence models truly predicted flow direction inside the cylinder. Their results also demonstrated that the nonlinear $k-\epsilon$ model predicted the energy amount of peak turbulent kinetics more than a linear model. Ibrahim and Makinde [12] have studied the effect of radiation on the MHD boundary layer through a porous vertical flat plate. Reddy et al. [13] investigated the effects of thermal radiation on the steady laminar flow of electrically conducting micropolar fluid past a stretching surface and observed that the skin-friction coefficient, heat and mass transference

decreases, and the gradient of angular velocity increases with an increase in porous medium inertia coefficient, inverse Darcy number, and magnetic field parameter. Ibrahim and Suneetha [14] analytically investigated the free convection heat transfer through a non-homogeneous porous medium bounded by an infinite porous vertical plate in slip flow regime while considering thermal radiation, chemical reaction, the Soret number, and heat source. Prakash et al. [15] studied the influence of porous medium and diffusion on the flow of unsteady viscous fluid over a vertical permeable surface considering thermal radiation and first-order chemical reaction.

Remie et al. [16] analytically derived the laminar flame impingement heat transfer and observed that the heatflux depends on the plate separation distance from the nozzle. Reddy and Sandeep [17] developed heat transfer characteristic of magneto-hydrodynamic free convective flow past a permeable rotating cone and a plate filled with gyrotactic microorganisms considering nonlinear thermal radiation and cross-diffusion. Wei et al. [18] experimentally investigated the impingement of laminar premixed biogas flame and found that with an increase in the velocity of unburnt gas, the heat flux and the total rate of heat transfer enhances significantly. Heat transfer properties of compressed natural gas were experimentally explored by Singh et al. [19]. They presented the distribution of radial temperature of flames for various operating conditions and at axial heights.

Nayak et al. [20] and [21] investigated natural convection heat transfer from heated vertical pipes experimentally and developed correlations for Nusselt number and Rayleigh number. Sahoo et al. [22] and [23] numerically studied the natural convection heat transfer from the vertical isothermal plate with protrusions and developed correlations to calculate the average Nusselt number as a function of fin spacing in the streamwise and spanwise directions, aspect ratio, and inclination of the fins. Gerdroodbari et al. [24] performed a numerical simulation to predict the outcome of micro air jets on the mixing of micro hydrogen jets in a supersonic flow. They

observed that when the number of air jets increases, the mixing performance of the fuel jet increases significantly. Amini et al. [25] investigated numerically the heat transfer taking swirling impinging jets and found that for $L/D = 6$ and 8 , the rate of heat transfer of swirling jets was more than regular jets, and the rate of heat transfer at higher Reynolds numbers increases due to a higher rate of momentum transfer. Gerdroodbari et al. [26], [27] numerically investigated the effect of angle of shock waves on transverse hydrogen micro-jets subjected to a supersonic crossflow focusing on mixing of hydrogen jet for high Mach number with an equivalence ratio of 0.5 . Gerdroodbari et al. [28] studied the thermal radiation effect on classical Jeffery–Hamel flow due to a point source or sink in convergent-divergent channels with stationary channel walls that are permitted to stretch or shrink. They observed that when the thermal radiation parameters increase, the temperature profile also increases. Fallah et al. [29] performed numerical simulations to analyse the influence of micro air jets on the mixing of fuel in the cavity flameholder of the scramjet and observed that mixing of fuel in the cavity improves significantly by the injection of fuel in the middle of the vertical wall.

2. Numerical solution

The physical model considered in the present work refers to a vertical flame jet impinging normally on a flat horizontal plate (Fig. 1). Diffusion flames generated by circular and annular jets are considered. The jet Reynolds number considered in this work refers to a steady, turbulent flame. RNG k- ϵ turbulent model is considered for analysis of turbulent flow in the flame.

The following assumptions are made in this analysis:

1. The flow is turbulent but steady (based on time mean values of flow parameters).
2. The irreversible two-step global reaction is considered for the oxidation of methane.
3. The gas phase comprising air and products of combustion is assumed to obey the ideal gas laws.

4. Flow at the outlet of the nozzle is considered to be uniform.

5. The system is considered to be a grey body with respect to radiation characteristics.

With all the above assumptions, the governing equations are given by:

Conservation of mass:

$$\nabla \cdot (\rho \vec{v}) = 0 \quad (1)$$

Conservation of momentum:

$$\rho [\vec{v} \cdot \nabla \vec{v}] = -\nabla p + \nabla \cdot (\mu_{eff} \nabla \vec{v}) + \vec{F}_B \quad (2)$$

$$\text{where } \mu_{eff} = \mu + \mu_t = \mu + \rho c_\mu \frac{k^2}{\varepsilon}$$

Here μ , μ_t , and μ_{eff} are the laminar, turbulent, and effective viscosities, respectively. \vec{F}_B is the gravitational body force.

Turbulent kinetic energy:

$$\nabla \cdot (\rho \vec{v} k) = \nabla \cdot \left(\frac{\mu_t}{\sigma_k} \nabla k \right) + G_k - \rho \varepsilon \quad (3)$$

Rate of dissipation of turbulent kinetic energy:

$$\nabla \cdot (\rho \vec{v} \varepsilon) = \nabla \cdot \left(\frac{\mu_t}{\sigma_\varepsilon} \nabla \varepsilon \right) + C_{1\varepsilon} \frac{\varepsilon}{k} G_k - \rho C_{2\varepsilon} \frac{\varepsilon^2}{k} \quad (4)$$

where k , ε , and G_k are the turbulent kinetic energy, rate of dissipation of turbulent kinetic energy, and generation of turbulent kinetic energy, respectively.

Conservation of energy:

$$\nabla \cdot (\rho \vec{v} h) = \nabla \cdot (\rho \alpha_{eff} \nabla h) - \nabla \cdot \vec{q}^r \quad (5)$$

$$\text{where } h = \sum_{k=1}^N Y_k [h_f^0 + \int_{T_{ref}}^T c_p k dT]$$

Here, h is the enthalpy of the mixture, h_f^0 is the enthalpy of formation, α_{eff} is the effective thermal diffusivity, and Y_k is the mass fraction of component k .

Species conservation:

$$\nabla \cdot (\rho \vec{v} Y_k) = \nabla \cdot (\rho D_{eff} \nabla Y_k) + S_k \quad (6)$$

Where D_{eff} and S_k represent effective mass diffusivity and source term for generation of k_{th} species, respectively.

Mass diffusivity for two species A and B is calculated by the empirical formula [30-31]

$$D_{AB} = \frac{0.00266 T^{3/2}}{PM_{AB}^{1/2} \sigma_{AB}^2 \Omega_D} \quad (7)$$

where M_A , M_B are molecular weights of A and B, respectively.

$$M_{AB} = 2 \left[\left(\frac{1}{M_A} \right) + \left(\frac{1}{M_B} \right) \right]^{-1} \quad (8)$$

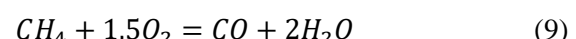
P is the pressure in bar

T is the temperature in K

$$\sigma_{AB} = \text{Characteristic length in \AA} = \frac{\sigma_A + \sigma_B}{2}$$

Chemical kinetics:

The equations for oxidation of methane are given by:



The rate of reaction is given by Magnussen and Hjertager [10], as given below:

Arrhenius equation:

$$\dot{\omega}_{fk} = B(\rho)^{a+b} \frac{Y_f^a Y_o^b}{M_f^a M_o^b} \exp \left(-\frac{E}{RT} \right) \quad (11)$$

Magnussen and Hjertager equation:

$$\dot{\omega}_{fd} = A \frac{\rho}{M_f k} \frac{\varepsilon}{\gamma} \left[\min \left(Y_f, \frac{Y_o}{\gamma}, \frac{c Y_P}{1+\gamma} \right) \right] \quad (12)$$

where M and γ are molecular weight and stoichiometric ratio, respectively.

Boundary conditions:

The flow field is assumed to be axisymmetric, and so, the computational domain is considered to be rectangular $-z$ -plane, as shown in Fig. 2. The boundary conditions considered for this analysis can be written in a cylindrical coordinate system as follows:

(i) At inlet ($z = 0$):

$$U_r = 0, U_z = U_{if}, T = T_i, Y_{CH4} = 1, Y_{O2} = 0,$$

where ($0 \leq r \leq r_b$),

$$U_r = 0, U_z = U_{ia}, T = T_i, Y_{CH4} = 0, Y_{O2} = 0.23,$$

where ($r_{b1} \leq r \leq r_{b2}$)

where r_{b1} refers to the inner radius, and r_{b2} refers to the outer radius of the nozzle.

(ii) At axis of symmetry ($r = 0$):

$$U_r = 0, \frac{\partial U_z}{\partial r} = \frac{\partial T}{\partial r} = \frac{\partial \rho}{\partial r} = \frac{\partial Y_k}{\partial r} = 0$$

(iii) At target plate ($z = H$):

No slip: $U_r = 0$,

No penetration: $U_z = 0$,

Isothermal: $T = T_w$

Impermeable: $\frac{\partial Y_k}{\partial z} = 0$

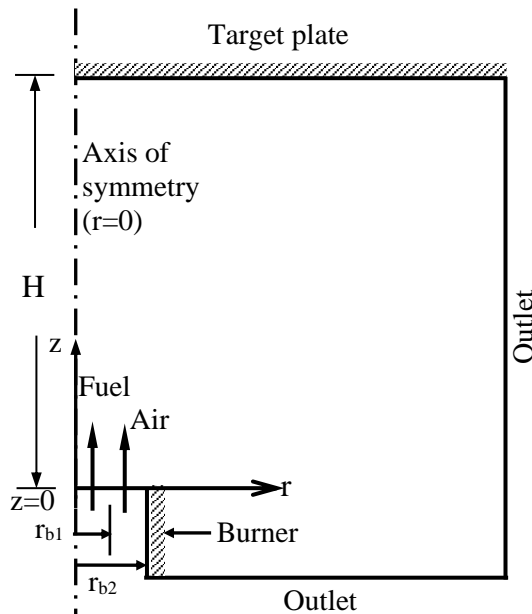


Fig. 2. Schematic diagram of computational domain.

(iv) Outlet:

$$\text{Radial direction: } \frac{\partial U_z}{\partial r} = \frac{\partial U_r}{\partial r} = \frac{\partial T}{\partial r} = \frac{\partial Y_k}{\partial r} = 0$$

$$\text{Axial direction: } \frac{\partial U_z}{\partial z} = \frac{\partial U_r}{\partial z} = \frac{\partial T}{\partial z} = \frac{\partial Y_k}{\partial z} = 0$$

(v) Nozzle wall:

$$\text{Adiabatic: } \left(\frac{\partial T}{\partial r}\right)_w = 0, \text{ or } \dot{q}_w = 0$$

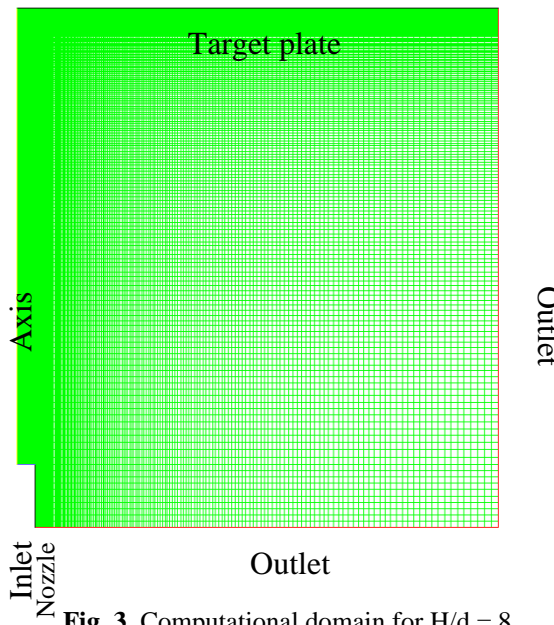


Fig. 3. Computational domain for $H/d = 8$.

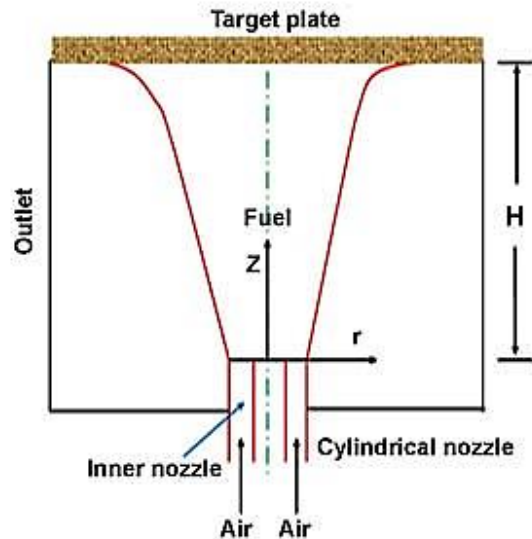


Fig. 4. Schematic diagram of diffusion flame impinging normally on plane surface.

3. Numerical solution procedures

In the present work, the conservation equations of mass, momentum, energy, turbulent kinetic energy, dissipation rate of turbulent kinetic energy, and species conservation equations are solved by employing a full time implicit finite volume technique using ANSYS Fluent software. SIMPLE algorithm is employed for pressure-velocity coupling. A second-order upwind scheme is used for discretizing

diffusion and advection terms. The convergence criteria for the residuals in all the discretized equations are set to 10^{-6} . A number of grids along the radial and axial directions are taken as 150 (r) \times 60 (z) to discretize for $H/d = 4$. For higher H/d ratios, the number of grids along the z-direction increases proportionately. For the numerical computations, methane is used as the fuel and the air is used as an oxidizer. For diffusion flame, the inner diameter of the nozzle for the flow of fuel is taken as $d_f = 4$ mm, and the outer diameter of the nozzle for the flow of air is taken as $d_a = 12$ mm. Temperature of fuel and air at the inlet is considered to be 300 K. The inlet velocities of air and fuel and separation distance of the target plate are varied to achieve the range of the following dimensionless input parameters:

(i) Jet Reynolds number, $Re = \frac{\rho U_i d}{\mu}$: 2000, 6000, 8000, 10000, 15000

(ii) Equivalence ratio, $ER = \frac{(Y_a/Y_f)_s}{(Y_a/Y_f)_a}$: 0.8, 1.0, 1.2, 2.0

where subscript s stands for stoichiometric, and a stands for actual air-fuel mixtures.

(iii) Ratio of distance of target plate and diameter of the nozzle, H/d : 4, 8, 12

For inlet velocity of fuel and air:

For fuel (methane) flow:

$d = 0.004$ m, at 300 K the kinematic viscosity = $17.28 * 10^{-6}$ m²/s, Since, $Re = \frac{\rho U_i d}{\mu}$

For $Re = 2000$, $U_{if} = 8.6$ m/s and for $Re = 15000$, $U_{if} = 64.8$ m/s

So for fuel flow, the velocity at inlet varies from 8.6 m/s to 64.8 m/s for the jet Reynolds numbers varying from 2000 to 15000.

Similarly for air flow:

$d = 0.008$ m (hydraulic diameter), at 300 K the kinematic viscosity = $4.765 * 10^{-5}$ m²/s, Since, $Re = \frac{\rho U_i d}{\mu}$

For $Re = 2000$, $U_{ia} = 11.91$ m/s, and for $Re = 15000$, $U_{ia} = 89.34$ m/s

So for air flow, the velocity at the inlet varies from 11.91 m/s to 89.34 m/s, for the jet Reynolds numbers varying from 2000 to 15000. T_i is taken as 300 K.

4. Results and discussion

In this analysis, an isothermal target plate of specified temperature is considered. The theoretical predictions of this model for the case of the premixed flame are compared with the experimental data of Vander Meer [1], as illustrated in Table 1. The theoretical results of the present model match closely with the experimental data.

For the grid independence test, several numerical experiments are conducted to determine the optimum number of grids along radial and axial directions.

Table 2 shows the variation of the average Nusselt number with a number of cells for various values of H/d for $Re = 6000$.

Fig. 5 depicts the dependence of the Nusselt number on grid size for various values of H/d . It is evident from Table 2 and Fig. 5 that for $H/d = 4$, as the number of grids in the domain increases from 3000 to 9000, the average Nusselt number changes from 175.20 to 260.45.

Table 1. Comparison of present theoretical predictions with experimental data [32].

Fixed input parameters	Variable parameters for both experimental (32) and present model		Nu (at stagnation point)
	H/d	Theoretical predictions by present model	
Fuel Methane	2	68.25	60.20
Premixed flame	4	112.10	103.25
$ER = 1.0$	6	116.50	108.40
$Re = 4226$	8	107.90	97.30

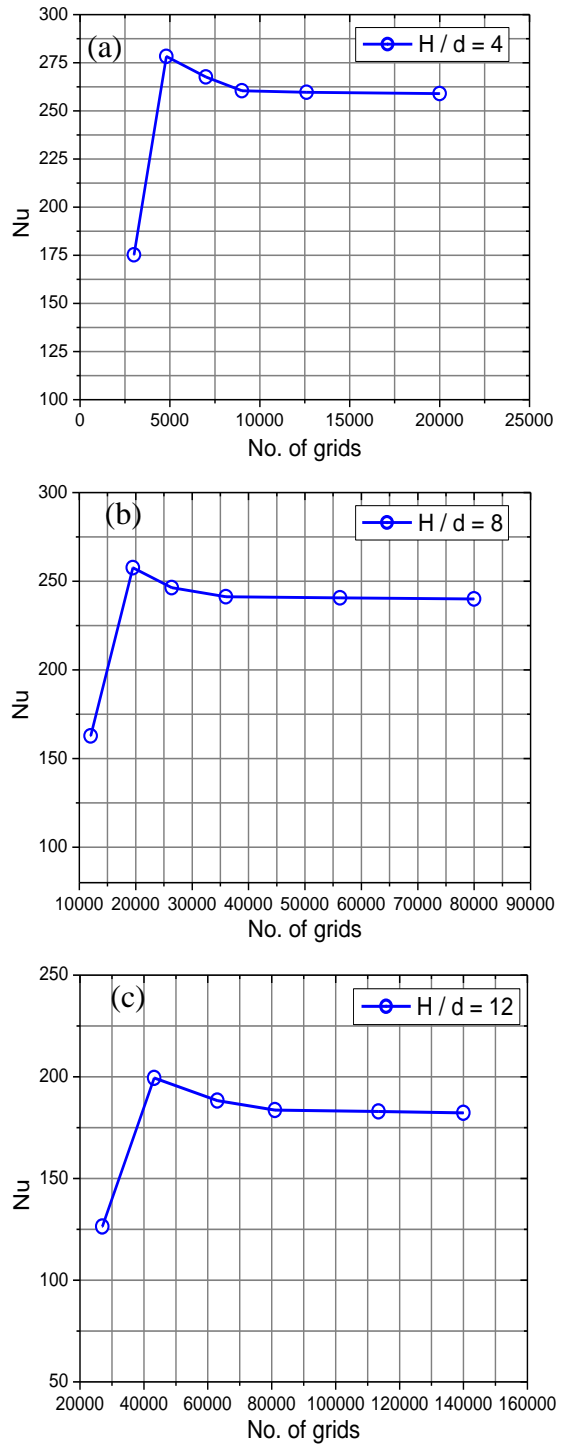
Table 2. Grid independence test.

	H/d = 4		H/d = 8		H/d = 12	
No.	No. of grids	Nu	No. of grids	Nu	No. of grids	Nu
1	3000	175.20	12000	162.75	27000	126.35
2	4800	278.32	19500	257.65	43200	199.45
3	7000	267.6	26400	246.32	63000	188.25
4	9000	260.45	36000	241.25	81000	183.68
5	12600	259.66	56250	240.65	113400	182.92
6	20000	258.95	80000	240.02	140000	182.25

Further increase in the number of grids up to 20000 has a negligible effect on the Nusselt number. Similarly, for H/d = 8, as the number of grids in the domain increases from 12000 to 36000, the average Nusselt number changes from 162.75 to 241.25. Further increase in the number of grids up to 80000 has a negligible effect on the average Nusselt number. And for H/d = 12, as the number of cells in the domain increases from 27000 to 81000, the average Nusselt number changes from 126.35 to 183.68. Further increase in the number of grids up to 140000 has almost no effect or negligible effect on the average Nusselt number.

Fig. 6 illustrates the distribution of heat flux at the surface of the plate for various values of H/d for $ER=1$ (based on the flow of air through the annular nozzle), and the fuel jet Reynolds number of 6000. The qualitative trends of heat flux distributions are almost the same as those in the case of premixed flame (Tripathy et al. [10]).

The main differences in the results with those of premixed flames are that the plate heat flux at any radial location for a given value of H/d is higher in diffusion flames. Heat flux increases significantly with a relatively flat distribution at the peak point. Similarly, the variation of heat flux at the plate surface for various values of H/d for $ER = 1$, and fuel jet $Re = 10000$ is given in Fig. 7.

**Fig. 5.** Average Nusselt number as a function of grid size for (a) H/d = 4, (b) H/d = 8, and (c) H/d = 12.

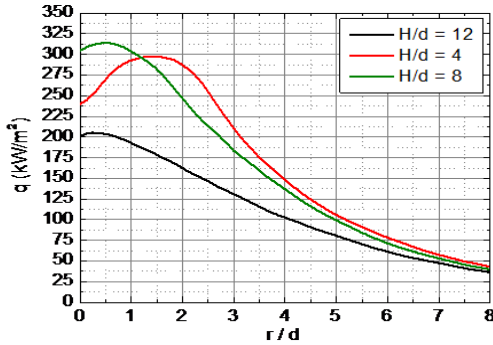


Fig. 6. Heat flux for various values of plate separation distance ($Re = 6000$, $ER = 1$).

It is evident from [Fig. 6](#) and [Fig. 7](#) that with an increase in the Reynolds number, the maximum heat flux increases for the same ER . For $H/d = 8$ with $Re = 6000$, the maximum heat flux of 315.99 kW/m^2 occurs at a radial distance $r/d = 0.49$, whereas for $H/d = 8$ with $Re = 10000$, the maximum heat flux of 337.61 kW/m^2 occurs at a radial distance $r/d = 0.69$.

Similarly, the heat flux distributions at the plate surface for various H/d , for $ER = 2$, and fuel jet $Re = 6000$ are depicted in [Fig. 8](#). It can be seen from [Figs. 6-8](#) that for $H/d = 12$, the maximum heat flux occurs very close to the center of the plate, and as H/d decreases the maximum heat flux region shifts slightly away from the center of the plate. For $Re = 6000$ and $ER = 1$, the maximum heat flux for $H/d = 4$ is 299.56 kW/m^2 and as H/d increases from 4 to 8, the maximum heat flux increases to 315.99 kW/m^2 . Further increasing the H/d ratio from 8 to 12, the maximum heat flux decreases to 205.86 kW/m^2 .

The gas phase temperature fields for diffusion flames for various H/d ratios are given in [Fig. 9-11](#). The diffusion flame under this situation is lifted from the burner and becomes relatively thinner with a more radial spread close to the plate surface as compared to the premixed flame (Tripathy et al. [10]). With the increase in the value of Re , the flame region gets more attached to the plate surface with a relatively larger radial spread of the flame. This results in higher heat fluxes at the plate surfaces. This may be due to the fact that the presence of the target plate spreads the flame in the radial direction when the velocity of the jet increases. For both $H/d = 4$ and 8, the flame appears to be a plate stabilized annular flame with an un-reacted cool central core ([Figs. 9](#) and [10](#)). This core extends up to a

distance very close to the plate surface for $H/d = 4$. This results in a relatively high-temperature zone in the stagnation region adjacent to the plate surface in the case of $H/d = 8$. For $H/d = 12$, the flame appears like a nozzle stabilized envelop which gets deflected by the plate ([Fig. 11](#)). Under this situation, there exists a short un-reacted burner attached cool conical core that is surrounded by an umbrella-like high-temperature flame zone that extends almost up to the plate surface.

When H/d increases, the flame temperature decreases due to the entrainment of more air from the surrounding. The heat flux in a stagnation region for $H/d = 12$ increases relatively with the peak value being close to that for $H/d = 8$. This may be because when the Reynolds number increases, the flame length also increases. [Fig. 12](#) depicts the variations of average Nusselt number over the plate with Re for different values of plate separation distance. It can be observed from [Fig. 12](#) that the average Nusselt number increases with the increase in Re .

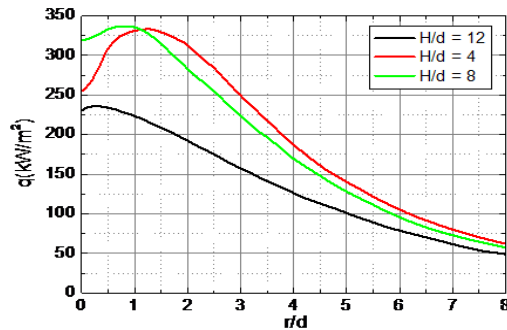


Fig. 7. Heat flux distributions for various plate separation distance ($Re = 10000$ and $ER = 1$).

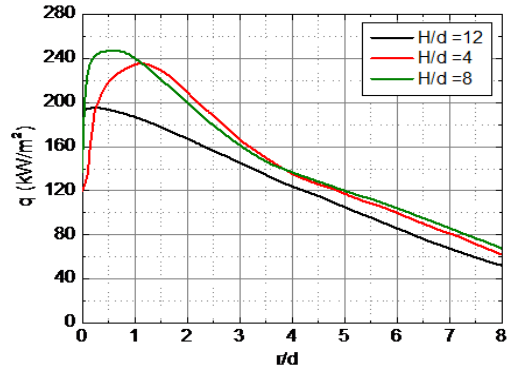


Fig. 8. Heat flux distributions for various plate separation distance ($Re = 6000$ and $ER = 2$).

The average Nusselt number \bar{Nu} also increases with a decrease in the value of H/d . The increase in the average Nusselt number is more pronounced for a change in H/d from 12 to 8 as compared to a change from 8 to 4 and that too in the higher range of Reynolds number. This can be attributed to the fact of having a more plate attached flame with lower values of H/d and at higher values of Re . Fig. 13 shows the dependence of average Nusselt number on the Reynolds number for various equivalence ratios (ER) with $H/d = 8$. The equivalence ratio varies from 1.0 to 2.0. It is evident that when ER increases, the average Nusselt number also increases. The increase in the value of \bar{Nu} with ER is more pronounced at higher values of Reynolds number (above $Re = 6000$). For a fuel-rich mixture of $ER=2$, a favorable zone of burning is formed near the plate due to entrainment of surrounding air, as a result of which the Nusselt number increases.

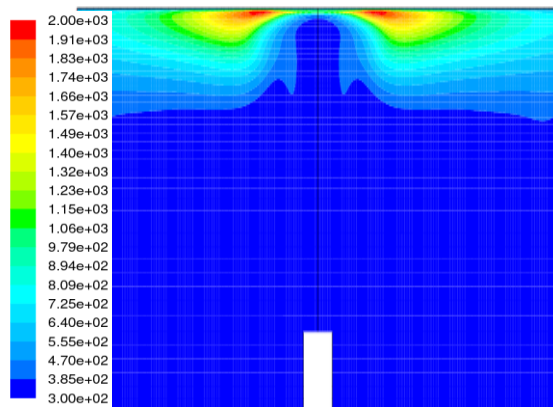


Fig. 9. Gas phase temperature fields for $H/d = 4$, $ER = 1$, and $Re = 6000$.

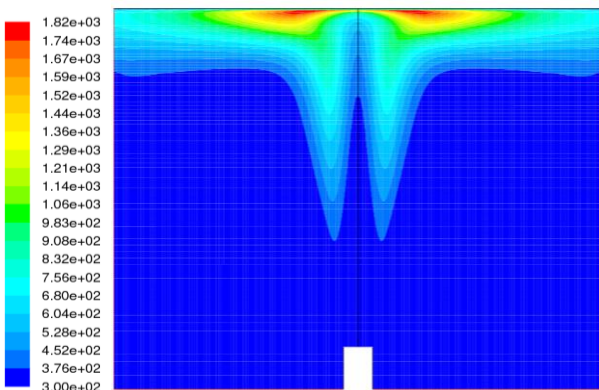


Fig. 10. Gas phase temperature fields for $H/d = 8$, $ER = 1$, and $Re = 6000$.

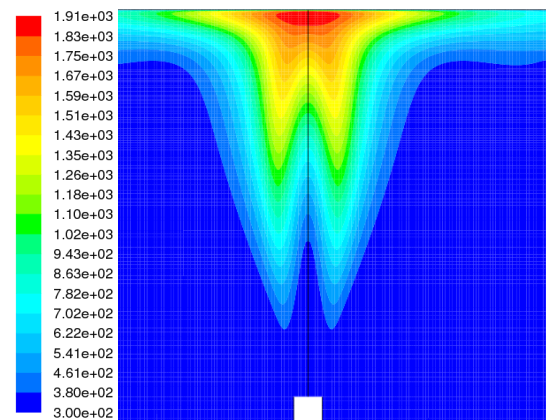


Fig. 11. Gas phase temperature fields for $H/d = 12$, $ER = 1$, and $Re = 6000$.

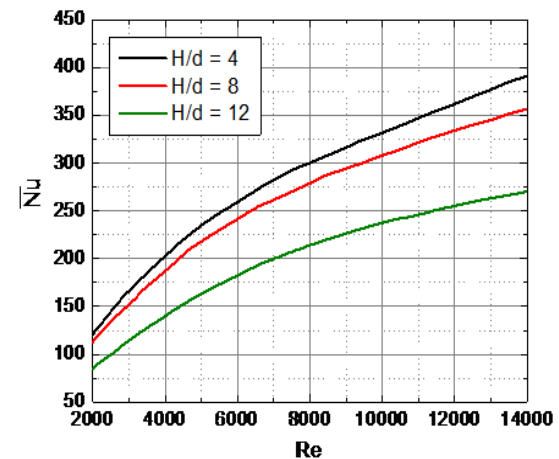


Fig. 12. Variations of average Nusselt number with Re for different values of H/d for $ER = 1$.

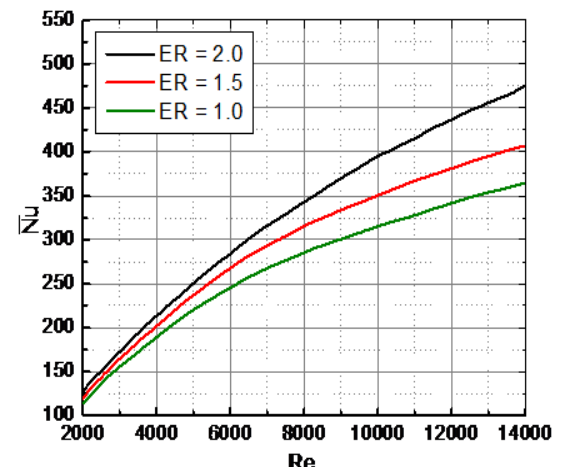


Fig. 13. Variations of average Nusselt number with Re for different values of ER for $H/d = 8$.

5. Conclusions

Theoretical analysis of turbulent diffusion flames impinging normally on plane surfaces has been developed to determine the average Nusselt number and the plate heat flux distribution as functions of jet Reynolds number, separation distance (H/d), and equivalence ratio (ER). The major observations made in this numerical study can be summarized as follows:

1. The peak value of heat flux occurs at a location slightly away from the stagnation point and gradually decreases away from the center of the plate.
2. The peak in the local heat flux comes closer to the stagnation point with an increase in the value of the separation distance of the plate from the nozzle.
3. Heat flux gradually increases with a decrease in the value of H/d from 12 to 8 but with a further decrease in the value of H/d from 8 to 4, it decreases.
4. When the Reynolds number increases, the average Nusselt number (\bar{Nu}) increases for all values of separation distance and equivalence ratio.
5. The average Nusselt number (\bar{Nu}) also increases with an increase in equivalence ratio (ER) for all values of plate separation distance, and the increase in the value of \bar{Nu} with ER is more prominent at higher values of Reynolds number (Re).

References

- [1] C. E. Baukal, and B. Gebhart, "A review of empirical flame impingement heat transfer correlations", *Int. J. Heat Fluid Flow*, Vol. 17, No. 4, pp.386-396, (1996).
- [2] Y. E. Boke, O. Aydin and H. D. Yildizay, "The Comparison of Experimental and Predicted Flame Temperature of Natural Gas Combustion", *Energy Sources, Part A: Recovery, Util. Environ. Eff.*, Vol. 33, No. 13, pp.1271-1280, (2011).
- [3] S. Chander, and A. Ray, "Heat transfer characteristics of laminar methane/air flame impinging normal to a cylindrical surface", *Exp. Therm. Fluid Sci.*, Vol. 32, No. 2, pp.707-721 (2007).
- [4] C. Cornaro, A.S. Fleischer, M. Rounds, and R. J. Goldstein, "Jet impingement cooling of convex semi-cylindrical surface", *Int. J. Therm. Sci.*, Vol. 40, No. 10, pp. 890–898, (2001).
- [5] L. L. Dong, C. S. Cheung, and C. W. Leung, "Heat transfer from an impinging premixed butane/air slot flame jet", *Int. J. Heat Mass Transfer.*, Vol. 45, No. 5, pp.979-992, (2002).
- [6] S. S. Hou, and Y. C. Ko, "Influence of oblique angle and heating height on flame structure temperature field and efficiency of an impinging laminar jet flame", *Energy Convers. Manage.*, Vol. 46, No. 6, pp. 941–958, (2005).
- [7] P. Kuntikana, and S. V. Prabhu, "Isothermal air jet and premixed flame jet impingement Heat transfer characterization and comparison", *Int. J. Therm. Sci.*, Vol. 100, pp. 401-415, (2016).
- [8] G. K. Agrawal, S. Chakraborty, and S. K. Som, "Heat transfer characteristics of premixed flame impinging upwards to plane surfaces inclined with the flame jet axis". *Int. J. Heat Mass Transfer*, Vol. 53, No. 9-10, pp. 1899–1907, (2010).
- [9] H. Lee, Y. S. Chung, and D. S. Kim, "Turbulent flow heat transfer measurement on curved surface with fully developed round impinging jet", *Int. J. Heat Fluid Flow*, Vol. 18, No. 1, pp. 60–169, (1997).
- [10] S. Tripathy, A. K. Rout, and M. K. Roul,"Heat Transfer due to Impinging Flame on Plane Surface", *Int. Organ. Sci. Res.*, Vol. 13, pp. 27-34, (2016).
- [11] A. Mirmohammadi, and F. Ommi, "Internal combustion engines in cylinder flow simulation improvement using nonlinear k- ϵ turbulence models", *J. Comput. Appl. Res. Mech. Eng.*, Vol. 5, No. 1, pp. 61-69, (2015).
- [12] S. Y. Ibrahim and O. D. Makinde, "Radiation effect on chemically reacting magneto hydrodynamics (MHD) boundary layer flow of heat and mass transfer through a porous vertical flat

- plate," *Int. J. Phy. Sci.*, Vol. 6, No. 6, pp. 1508-1516, (2011).
- [13] L. R. Reddy, M. C. Raju, G. S. S. Raju and S. M. Ibrahim, "Chemical reaction and thermal radiation effects on MHD micropolar fluid past a stretching sheet embedded in a non-Darcian porous medium", *J. Comput. Appl. Res. Mech. Eng.*, Vol. 6, No. 2, pp. 27-46, (2016).
- [14] S. Mohammed Ibrahim and K. Suneetha, "Effects of thermal diffusion and chemical reaction on MHD transient free convection flow past a porous vertical plate with radiation, temperature gradient dependent heat source in slip flow regime", *J. Comput. Appl. Res. Mech. Eng.*, Vol. 5, No. 2, pp. 83-95, (2015).
- [15] J. Prakash, P. Durga Prasad, R. V. M. S. S. Kiran Kumar and S. V. K. Varma, "Diffusion-thermo effects on MHD free convective radiative and chemically reactive boundary layer flow through a porous medium over a vertical plate", *J. Comput. Appl. Res. Mech. Eng.*, Vol. 5, No. 2, pp. 111-126, (2015).
- [16] M. J. Remie, M.F.G. Cremers, K. R. A. M. Schreel and L.P.H. de Goey, "Analysis of the heat transfer of an impinging laminar flame jet", *Int. J. Heat Mass Transfer*, Vol. 50, No. 13-14, pp. 2816-2827, (2007).
- [17] M. Gnaneswara Reddy, and N. Sandeep, "Free convective heat and mass transfer of magnetic bio-convective flow caused by a rotating cone and plate in the presence of nonlinear thermal radiation and cross diffusion", *J. Comput. Appl. Res. Mech. Eng.*, Vol. 7, No. 1, pp. 1-21, (2017).
- [18] Z. L. Wei, H. S. Zhen, C. W. Leung, C. S. Cheung and Z.H. Huang, "Heat transfer characteristics and the optimized heating distance of laminar premixed biogas hydrogen Bunsen flame impinging on a flat surface", *Int. J. Hydrogen Energy*, Vol. 40, No. 45, pp. 15723-15731, (2015).
- [19] G. Singh, S. Chander and A. Ray, "Heat transfer characteristics of natural gas/air swirling flame impinging on a flat surface", *Exp. Therm. Fluid Sci.*, Vol. 41, pp. 165-176, (2012).
- [20] R. C. Nayak, M. K. Roul, and S. K. Sarangi, "Experimental Investigation of Natural Convection Heat Transfer in Heated Vertical Tubes with Discrete Rings", *Exp. Tech.*, Vol. 41, No. 6, pp. 585-603, (2017).
- [21] R. C. Nayak, M. K. Roul, and S. K. Sarangi, "Natural Convection Heat Transfer in Heated Vertical Tubes with Internal Rings." *Arc. Thermodyn.*, Vol. 39, No. 4, pp. 85-111, (2018).
- [22] L. K. Sahoo, M. K. Roul, and R. K. Swain, "Natural convection heat transfer augmentation factor with square conductive pin fin arrays", *J. Appl. Mech. Tech. Phys.*, Vol. 58, No. 6, pp. 1115-1122, (2017).
- [23] L. K. Sahoo, M. K. Roul, and R. K. Swain, "CFD Analysis of natural convection heat transfer augmentation from square conductive horizontal and inclined pin fin arrays", *Int. J. Ambient Energy*, Vol. 39, pp. 840-851, (2018).
- [24] M. B. Gerdroodbar, M. Mokhtari, K. Fallahand H. Pourmirzaagha, "The influence of micro air jets on mixing augmentation of transverse hydrogen jet in supersonic flow", *Int. J. Hydrogen Energy*, Vol. 41, No. 47, pp. 22497-22508, (2016).
- [25] Y. Amini, M. Mokhtari, M. Haghshenasfard and M. B. Gerdroodbar, "Heat transfer of swirling impinging jets ejected from Nozzles with twisted tapes utilizing CFD technique", *Case Stud. Therm. Eng.*, Vol. 6, pp.104-115, (2015).
- [26] M. B. Gerdroodbar, O. Jahanianand M. Mokhtari, "Influence of the angle of incident shock wave on mixing of transverse hydrogen micro-jets in supersonic crossflow", *Int. J. Hydrogen Energy*, Vol. 40, No. 30, pp. 9590-9601, (2015).
- [27] M. B. Gerdroodbar, D. D. Ganji and Y. Amini, "Numerical study of shock wave interaction on transverse jets through multiport injector arrays in supersonic

- crossflow", *Acta Astronaut.*, Vol. 115, pp. 422-433, (2015).
- [28] M. B. Gerdroodbary, M. Rahimi Takami and D.D. Ganji, "Investigation of thermal radiation on traditional Jeffery–Hamel flow to stretchable convergent/divergent channels", *Case Stud. Therm. Eng.*, Vol. 6, pp. 28-39, (2015).
- [29] K. Fallah, M. B. Gerdroodbary, A. Ghaderi and J. Alinejad, "The influence of micro air jets on mixing augmentation of fuel in cavity flame holder at supersonic flow", *Aerosp. Sci. Technol.*, Vol. 76, pp.187-193, (2018).
- [30] B. E. Poling J. M. Prausnitz and J. P. O'Connell, *The Properties of Gases and Liquids*, 5th ed., McGraw Hill Book Company, New York, (2001).
- [31] F. Magnussen, and B. H. Hjertager, "On mathematical modelling of turbulent combustion with specified emphasis on soot formation and combustion", *combust. Inst. Cambridge USA*, Vol. 16, No. 1, pp. 719-729, (1977).
- [32] T. H. Vander Meer, "Stagnation point heat transfer from turbulent low Reynolds number jets and flame jets". *Expt. Therm. Fluid Sci.* Vol. 4, No. 1, pp. 115-126, (1991).

Copyrights ©2021 The author(s). This is an open access article distributed under the terms of the Creative Commons Attribution (CC BY 4.0), which permits unrestricted use, distribution, and reproduction in any medium, as long as the original authors and source are cited. No permission is required from the authors or the publishers.



How to cite this paper:

SatyanandaTripathy, Manmatha K. Roul, Akshaya Ku. Rout, "Heat transfer characteristics of methane-air diffusion flames impinging normally on plane surfaces", *J. Comput. Appl. Res. Mech. Eng.*, Vol. 10, No. 2, pp. 361-372, (2021).

DOI: 10.22061/jcarme.2019.3962.1466

URL: https://jcarme.sru.ac.ir/?_action=showPDF&article=1067

